(This is a sample cover image for this issue. The actual cover is not yet available at this time.)

Remote Sensing of Environment 130 (2013) 266–279

Contents lists available at SciVerse ScienceDirect

Remote Sensing of Environment

journal homepage: www.elsevier.com/locate/rse

Comparison of methods for estimation of absolute vegetation and soil fractional cover using MODIS normalized BRDF-adjusted reflectance data

Gregory S. Okin [a,*], Kenneth D. Clarke [b], Megan M. Lewis [b]

[a] Department of Geography, University of California, Los Angeles, CA 90095, United States
[b] School of Earth and Environmental Sciences, The University of Adelaide, Adelaide 5005, Australia

ARTICLE INFO

Article history:
Received 28 March 2012
Received in revised form 4 November 2012
Accepted 13 November 2012
Available online xxxx

Keywords:
Remote sensing
MODIS
Vegetation indices
Nonphotosynthetic vegetation
Fractional cover
Soil
Field spectroscopy
Validation

ABSTRACT

Green vegetation (GV), nonphotosynthetic vegetation (NPV), and soil are important ground cover components in terrestrial ecosystems worldwide. There are many good methods for observing the dynamics of GV with optical remote sensing, but there are fewer good methods for observing the dynamics of NPV and soil. Given the difficulty of remotely deriving information on NPV and soil, the purpose of this study is to evaluate several methods for the retrieval of information on fractional cover of GV, NPV, and soil using 500-m MODIS nadir BRDF-adjusted reflectance (NBAR) data. In particular, three spectral mixture analysis (SMA) techniques are evaluated: simple SMA, multiple-endmember SMA (MESMA), and relative SMA (RSMA). In situ cover data from agricultural fields in Southern Australia are used as the basis for comparison. RSMA provides an index of fractional cover of GV, NPV, and soil, so a method for converting these to absolute fractional cover estimates is also described and evaluated. All methods displayed statistically significant correlations with in situ data. All methods proved equally capable at predicting the dynamics of GV. MESMA predicted NPV dynamics best. RSMA predicted dynamics of soil best. The method for converting RSMA indices to fractional cover estimates provided estimates that were comparable to those provided by SMA and MESMA. Although it does not always provide the best estimates of ground component dynamics, this study shows that RSMA indices are useful indicators of GV, NPV, and soil cover. However, our results indicate that the choice of unmixing technique and its implementation ought to be application-specific, with particular emphasis on which ground cover retrieval requires the greatest accuracy and how much ancillary data is available to support the analysis.

1. Introduction

Vegetation dynamics has emerged as an important topic with relevance to a wide array of climate and ecological research including regional and global carbon modeling, ecological assessment, and agricultural monitoring, to name only a few (Asner et al., 2000; Lucht et al., 2002; Parmesan and Yohe, 2003). At the ecosystem-level, there is significant history of the use of remotely-derived vegetation indices to monitor vegetation (e.g., Jia et al., 2003; Reed, 2006; Reed et al., 1994; Tucker et al., 1991; Zhang et al., 2003, 2006). Common multispectral vegetation indices, such as the normalized difference vegetation index (NDVI, Tucker, 1979) and the enhanced vegetation index (EVI, Huete et al., 2002), exploit the difference in visible and near-infrared (NIR) reflectance due to the presence of chlorophyll. These indices only provide information about the green (or photosynthetic) portion of terrestrial vegetation.

Though green vegetation (GV, sometimes also called photosynthetic vegetation, PV) is undoubtedly a critical component of vegetation dynamics, it is not the only component. Nonphotosynthetic vegetation (NPV), whether standing live material, standing senescent material, or litter is a key element of many terrestrial ecosystems (e.g., Asner and Heidebrecht, 2002; Elmore et al., 2005; Guerschman et al., 2009; Roberts et al., 1993). For instance, NPV provides vertical structure in ecosystems, large amounts of carbon is stored in living and dead NPV, and NPV (particularly dead) is susceptible to fire. Bare ground cover is a critical element of terrestrial ecosystems as well, with important controls on albedo and erosion (e.g., Balling, 1988; Bonfils et al., 2001; Kleidon et al., 2000; Lopez et al., 2000; Nicholson, 2000; Warren and Hutchinson, 1984).

Thus, value can be added to remote sensing studies of the Earth's ecosystems by incorporating information on NPV dynamics. The cellulose absorption index (CAI) (Nagler et al., 2003) has been suggested as one method, though this approach relies on several relatively narrow spectral bands in the short-wave infrared (SWIR) that are usually provided by hyperspectral imagery. To date, there are few methods for retrieval of NPV dynamics from multispectral imagery. Guerschman et al. (2009) found that a combination of NDVI and a ratio of moderate resolution imaging spectrometer (MODIS) reflectance bands could be empirically calibrated against CAI values to yield time series of NPV cover that showed agreement with field data. This approach is not theoretically based.

* Corresponding author. Tel.: +310 825 1071.
E-mail address: okin@ucla.edu (G.S. Okin).

0034-4257/$ – see front matter © 2012 Elsevier Inc. All rights reserved.
http://dx.doi.org/10.1016/j.rse.2012.11.021

One problem with the retrieval of NPV cover information from coarse spectral resolution remote sensing data is its spectral similarity to soil; the spectral variance of these two endmembers overlaps (Okin, 2007). In the visible and NIR portions of the spectrum, both typically have increasing reflectance with increasing wavelength with few strong spectral absorption features. In the SWIR spectral region from 2 to 2.5 μm, NPV and soil can have distinctive absorption features that can be discerned using high spectral resolution. In NPV, these are due to C–H, N–H, and C–O vibrations in starches and sugars (Curran, 1989) and in soils these are typically due to Al-OH or metal-OH vibrations in minerals (Clark et al., 1990). However, these features, as well as the tendency of absorption to decrease in both minerals and NPV with increasing wavelength in the SWIR, mean that it can be difficult to separate soil and NPV using coarse spectral resolution imagery such as MODIS or TM/ETM + without knowledge of at least one component. In contrast, the characteristic spectrum of GV with strong absorption in the visible, high reflectance in the NIR and characteristic water absorption features throughout the infrared makes GV easy to separate spectrally from both NPV and soil (Curran, 1989). The usual strong difference in reflectance between the red and NIR wavelengths is the basis of many indices of GV cover that can be used with coarse spectral resolution data (e.g., Huete et al., 2002).

Spectral mixture analysis (SMA) and its derivatives provide another promising avenue for retrieval of NPV and soil cover from multispectral imagery (e.g., Asner and Heidebrecht, 2002; Ballantine et al., 2005; Elmore et al., 2005), however most SMA techniques require knowledge of the spectrum of the soil background. The spectra of soils, in turn, are highly diverse depending on mineral content, organic matter content, soil texture, and the presence of crusts (e.g., Ben-Dor and Banin, 1994; Ben-Dor et al., 2003; Chabrillat et al., 2002; Franklin et al., 1993; Gerbermann, 1979; Karnieli et al., 1999; Okin and Painter, 2004; Palacios-Orueta and Ustin, 1998; Price, 1990). The resultant spatial variability of soil spectra makes large-scale SMA-based analysis in which knowledge of the soil spectrum is required extremely difficult. Multiple endmember SMA (MESMA, Roberts et al., 1998) was developed to accommodate spectral variability in all ground components, including soil, but requires a large library of endmember spectra. In contrast, relative spectral mixture analysis (RSMA, Okin, 2007) was designed to obviate the need for a library of soil endmembers, or indeed any soil endmember, while still providing information on the dynamics of GV, NPV, and soil.

Given the difficulty of deriving information on the fractional cover of NPV and soil, the purpose of this report is to determine how SMA-based indices of GV, NPV, and soil derived from 500-m MODIS reflectance data perform in relation to in situ fractional cover measurements. Because RSMA differs from the other SMA-based methods we also describe and evaluate a method for calibrating RSMA-based indices to absolute fractional cover.

2. Methods

2.1. Study area

The study was conducted in a rain-fed cropping region of South Australia with a Mediterranean climate (Fig. 1). The region experiences hot dry summers (December–February) and mild wet winters (July–August), and receives an average annual rainfall of approximately 500 mm. Agriculture in the region is dominated by annual rotations of cereal crops, legumes and rapeseed/canola (*Brassica napu*). Through the summer, the landscape is largely dry although out of season rainfall can lead to summer weed and pasture growth that can produce significant GV cover. This is followed by rainfall in late March through to May and subsequent weed and pasture growth, until chemical spraying of weeds and seeding, or direct-drill seeding, which reduce cover to a minimum in May–June. Following seeding, annual crops germinate and growth peaks in September. Finally crops ripen, senesce and are harvested in November and December. Stubble remaining after harvest is commonly grazed by stock throughout summer.

This study focuses on nine fields ranging in size from 61 to 257 ha. These fields were chosen for their extremely large size, relative uniformity of soil and uniformly flat topography. This design allowed us to obtain fractional cover from fields corresponding to several MODIS pixels, with reasonable expectation of homogenous soil-cover due to minimal soil variability and minimal topographic redistribution of rainfall.

2.2. In situ fractional cover data

In situ fractional cover data were collected on three dates using two survey methods, one step-point and the other photographic (Table 1). Three dates were sampled to ensure that a wide range of fractional covers (i.e., f_{GV}, f_{NPV} and f_{Soil}) were characterized. The April and June survey dates were chosen to capture maximum f_{Soil}. The October survey was timed to coincide with the expected time of peak green canopy cover, but before any crop senescence, to capture maximum f_{GV}.

The step-point method was used on the first two survey dates (April and June) when crops were either not present, or were so new that little damage was caused. The photographic method was used on the last field survey dates when crop canopies were full and green (October). The photographic method was used to minimize crop disturbance.

2.2.1. Step-point method

To record in situ fractional cover with our step-point method two surveyors walked step-point transects (Evans and Love, 1957; Mentis, 1981) crossing each field from fence to fence in a "W" pattern. Both surveyors started in the middle of "W" in the middle of one side fence, and each walked half of the "W", reaching the opposite fence at the 1/3rd and 2/3rd points, then returning towards the starting side and finishing in the field corners. On every second step (~1.5-m intervals) surveyors recorded the cover type (GV, NPV or soil) directly under a thin line drawn on the end of their shoe. For each field, fractional cover was determined by combining the step-point tallies of both surveyors, and then calculating the proportion of each cover type out of the combined tallies. The total number of step-point recordings taken within each field ranged from ~560 to 2500 depending on field size.

2.2.2. Photographic method

Vertical, nadir-oriented high-resolution color digital photographs were taken from approximately 1 m above the crop canopy. In situ fractional cover was determined by overlaying a regular grid of 100 points (10 × 10) over each photograph, and visually scoring the cover type at each point as GV, NPV, soil or shadow/unidentified. For each field, fractional cover was determined by combining the point tallies from all photographs for that field, excluding shadow/unidentified, and calculating the proportion of each cover type out of the total tally for that field.

Between six and thirty photographs were taken in each field to ensure that within-field variability was adequately captured. Photographs were taken near the corner of each field, far enough into the crop that no edge effects were visible. If some field corners were not accessible, they were not sampled. At each corner a short transect was walked into the field and a photograph was taken every five paces. In fields with more perceived cover variation more photographs were taken. However, analysis revealed little variation in cover levels between photographs within each field. The total number of points assessed from all photographs for each field ranged from 600 to 2500.

2.2.3. Comparison of step-point and photographic method

While the step-point and photographic methods differ, these differences should not have differentially influenced the measured vegetation

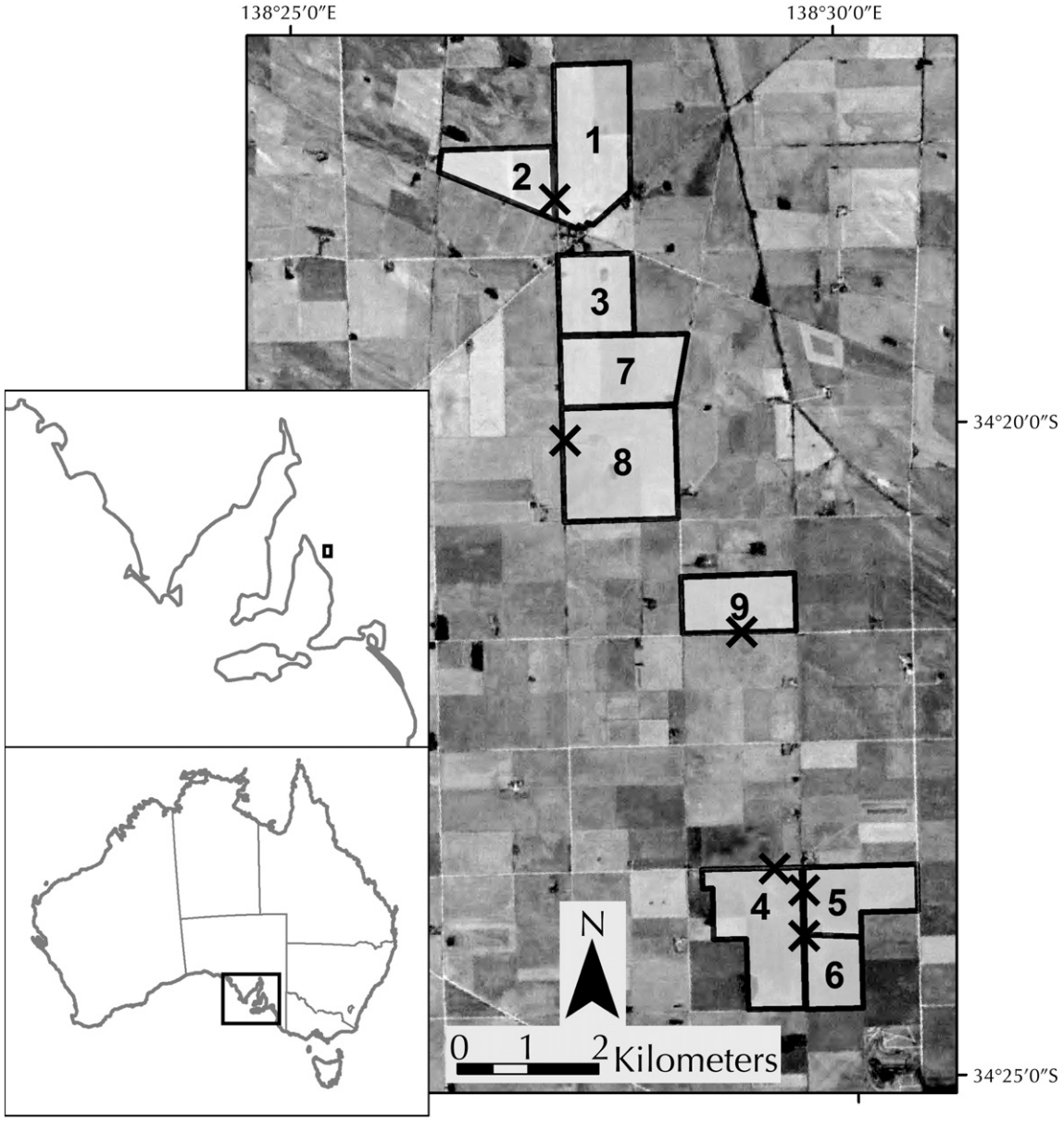

Fig. 1. Study site. Fields numbered 1–9 were used in this study. The locations where field spectra were acquired are marked with "X".

cover fractions. Both methods relied on human visual interpretation of cover type at points, and both methods were designed to minimize user bias in point placement.

2.3. Field spectroscopy

Despite the relative uniformity of soils in the study area, soils were still expected to account for the majority of within-scene spectral variation, with little variation in GV and NPV spectra. To this end, field spectral collection primarily focused on capturing the range of present soil spectral variation, and secondarily captured some reference GV and NPV spectra.

Spectra were collected in the field with an Analytical Spectral Devices (ASD) full-range Fieldspec® 4 spectroradiometer (wavelength range 400–2500 nm) contact probe. Prior to the first spectra collection at each site, and when switching from one cover type to another at a site the spectroradiometer was optimized and then calibrated to a Spectralon® white reference target.

Field spectra were recorded on 21 March 2011, and between 4 and 11 soil spectra were recorded at each of nine locations covering the two major soil groups present in the study fields (Fig. 2). Between five and seven NPV spectral samples were collected for each of the three crop residues present in the study fields (lentils, rapeseed and wheat). As the spectral sampling was conducted very early in the growing season the only green vegetation present was wheat. Three green wheat spectra were recorded.

Table 1
Field survey dates, MODIS NBAR data composite dates (MODIS production period), and survey method. All dates are 2010.

Field survey	MODIS NBAR composite dates (production period)	Survey method
27-Apr	April 23–May 8 (2010113)	Step-point
22-Jul	July 12–July 27 (2010193)	Step-point
8-Oct	September 30–October 15 (2010273)	Photographic

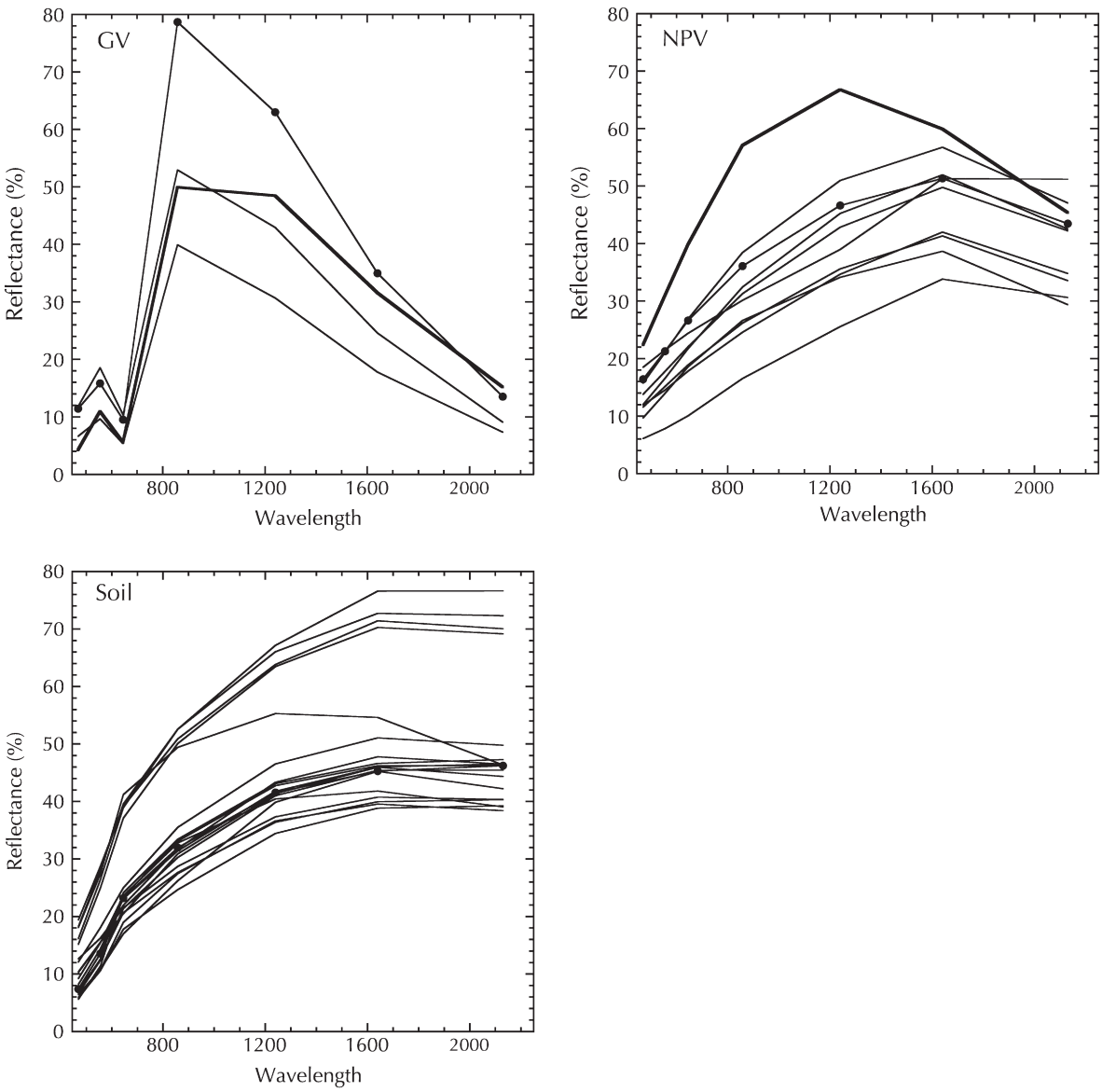

Fig. 2. Reflectance spectra used as endmembers in RSMA, SMA, and MESMA unmixing of MODIS NBAR data. The heavy lines are the RSMA endmember spectra (RSMA does not use a soil endmember), the filled circles are the SMA endmembers, and the thin lines are the MESMA endmembers. For clarity, only one-half of MESMA soil endmembers are shown here. SMA and MESMA endmembers are derived from field spectroscopy.

2.4. Remote sensing

2.4.1. MODIS data

Two MODIS datasets were used in this study. The first was the Terra + Aqua 500-m, 16-day MODIS Nadir BRDF-adjusted reflectance (NBAR) dataset (MCD43A4, NASA Land Processes Distributed Active Archive Center (LP DAAC), 2001a; Schaaf et al., 2002). The second was the Terra 500-m 16-day MODIS vegetation index dataset (MOD13A1, NASA Land Processes Distributed Active Archive Center (LP DAAC), 2001b; Huete et al., 2002), from which EVI values were extracted. The compositing dates for both datasets are given in Table 1. Average values for each field for EVI for each compositing period were extracted for comparison with other estimates of GV dynamics.

2.4.2. SMA and MESMA

In SMA, the apparent surface reflectance is assumed to be a linear combination of the reflectance of the spectra of the ground components, "endmembers", weighted by their fractional cover in each pixel. The SMA equation for n endmembers at time t_i is:

$$\rho_{\text{pixel}}^{t_i} = \sum_{k=1}^{n} f_k^{t_i} \rho_k + \varepsilon, \tag{1}$$

where $\rho_{\text{pixel}}^{t_i}$ is the reflectance of the pixel at time t_i, ρ_k is the reflectance of the k-th endmember, and $f_k^{t_i}$ is the fractional area covered by the k-th endmember at time t_i (Shimabukuro and Smith, 1991). When derived from laboratory or field spectra, ρ_k are sometimes called "reference endmembers" (Roberts et al., 1998). The final term, ε, is the residual spectrum remaining after best-fit coefficients, $f_k^{t_i}$, have been determined. Eq. (1) is sometimes subject to the constraints that f_k must belong to the interval [0,1] and

$$\sum_{k=1}^{n} f_k^{t_i} = 1. \tag{2}$$

SMA assumes that the reference endmembers are spatially invariant. Use of SMA in the context here, where the same endmembers are used to unmix images from different times further requires the assumption that the endmembers are temporally invariant.

MESMA is a version of SMA in which the best-fit coefficients of many different SMA models (a model is a unique combination of endmember spectra) are calculated and the best model is picked among these (Roberts et al., 1998). One criterion often used in MESMA to pick the best model is $RMSE_S$:

$$RMSE_S = \left(\frac{1}{m}\sum_{b=1}^{m}(\varepsilon_b)^2\right)^{1/2} \quad (3)$$

where m is the number of bands in the remote sensing imagery (MCD43A4 has seven bands) and the subscript 'S' refers to the RMSE of the spectral fit; the model with the lowest $RMSE_S$ is chosen (Roberts et al., 1998). For applications with a large number of bands, such as those using hyperspectral data, other criteria can be used (e.g., Dennison et al., 2004; Roberts et al., 1997). Endmember spectra used for MESMA analysis are shown in Fig. 2. Collection of field spectra used as endmembers for MESMA is discussed above. Models were constructed by using all possible combinations among three GV spectra, nine NPV spectra, and 38 soil spectra resulting in 1026 total models.

Examination of the MESMA results for the area containing our fields showed that only three models were used to model the field area, with one model being by far the dominant. All of these models contained the same GV and NPV spectra and differed only in their soil spectra. The GV and NPV spectra that were used by MESMA in the best models of our fields were used as endmembers in the SMA unmixing as was the soil spectrum from the dominant model (Fig. 2).

Any spectrum can be used as an endmember, though each cover type can be represented only once, and we wished to use the most spectrally representative field spectra in our SMA unmixing. Given the high variability in measured field spectra even over a small area, no endmember spectrum can be identified as the most representative ab initio, particularly in light of the impact of vegetation structure on what MODIS ultimately sees. The use of the spectra that resulted in the lowest residual error, in a set of MESMA models where all combinations are tried, guarantees that SMA will provide the lowest possible residual errors as well. However, selection of SMA endmembers in this way probably optimizes the ability of SMA to capture fractional cover, compared to an approach where SMA endmembers are chosen without guidance based on how well they fit the image spectra.

For both SMA and MESMA, unmixing was conducted using the "constrained_min" routine in IDL (Excelis Visual Information Solutions, Inc., Boulder, Colorado; Lasdon and Waren, 1986) to minimize RMSE while forcing coefficients to exist in the interval [0,1]. The advantage to this approach compared to another linear unmixing method using linear algebraic least-squares analysis (including a QR decomposition using the Gram–Schmidt process or the use of singular value decomposition (SVD)) is that constraints can be strictly enforced; values outside [0,1] can be avoided if desired. Roberts et al. (1998), using a least-squares mixing approach based on a QR decomposition using Gram–Schmidt orthogonalization, for instance, allowed endmembers to be slightly outside the [0,1] constraints. In cases where there exists a solution for the endmembers that falls within the constraints, both the method used here and a linear algebraic least-squares will provide the same solution.

Two sets of SMA and MESMA fractional cover estimates were included in our analysis. In the first, no constraint on the sum of non-shade endmembers was imposed. This method is equivalent to that used in Roberts et al. (1998). In that study, the constraint that all endmembers sum to one is imposed by inferring an additional photometric shade endmember (zero reflectance in all bands) that is not used in the actual unmixing. The fractional cover of the photometric shade endmember is set to one minus the sum of the other endmember fractions. This approach is required because photometric shade cannot be used directly as an endmember in a spectral mixture model. Depending on the algorithm used for estimation of fractions (i.e., f_k,) several undesirable outcomes result with the inclusion of photometric shade directly. For instance: 1) using simple linear least squares, the X^TX matrix, where X is a column vector containing endmembers, is not invertible, 2) a least squares approximation using QR decomposition employing the Gram–Schmidt process results in non-real Q and R matrix values, 3) least squares estimation using singular value decomposition (SVD) results in the shade fraction always being equal to zero, and 4) the heuristic constrained_min algorithm based on gradient reduction used here results in unstable shade fractions (i.e., subsequent calculations do not result in the same shade fraction). In the first two cases, the failure occurs because the photometric shade is a linear combination of any/all of the other spectra through multiplication by zero, a condition that is prohibited in these methods.

In the second set of fractional cover estimates, best-fit coefficients for a pixel were divided by the sum of all best-fit (non-shade) coefficients for that pixel, thus ensuring that the fractional cover estimates summed exactly to one. This method more closely matches treatment of in situ data, in which the sum of GV, NPV, and soil points were used to normalize GV, NPV and soil fractions, thus ignoring shade points.

2.4.3. RSMA

As originally published, RSMA used four endmembers to unmix pixel spectra: a baseline spectrum, a GV spectrum, an NPV spectrum, and a snow spectrum (Okin, 2007). Since snow does not fall in the study area the snow endmember was omitted from this analysis. In RSMA, the apparent surface reflectance for a pixel at a reference time, t_o, in a timeseries of collocated images is defined as the "baseline" spectrum of that pixel, ρ_B. From Eq. (1), the baseline spectrum can be modeled (assuming, in this case, no snow) as:

$$\rho_B = f_{GV}^{t_o}\rho_{GV} + f_{NPV}^{t_o}\rho_{NPV} + f_{soil}^{t_o}\rho_{soil}. \quad (4)$$

The reflectance of the soil background, ρ_{soil}, is assumed to vary spatially and is assumed to be unknown. $f_{GV}^{t_o}$, $f_{NPV}^{t_o}$, and $f_{soil}^{t_o}$ (i.e., the fractional area of the ground components at time t_o) are also assumed to be unknown. The spectra of the ground components, ρ_{GV}, ρ_{NPV}, and ρ_{soil}, are assumed to be invariant with time.

The assumption that the soil spectrum is constant with time over a MODIS pixel and compositing period is justifiable, particularly in arid areas. In a sandy soil, light from the sun only penetrates about four sand grains (i.e. a few millimeters) into the soil (Okin et al., 2001). In heavier textured soils, this distance will be smaller due to more efficient scattering by small particles (Hapke, 1981). Thus, though soil moisture does reduce soil reflectance by changing the index of refraction of the medium in soil pores, once the top several particles are back into equilibrium with the (dry) atmosphere, reflectance will return to its pre-wetting value (Lobell and Asner, 2002). This happens in arid areas, including our field site, quite quickly after wetting. A back of the envelope calculation using the data of Lobell and Asner (2002) assuming a constant evaporation equal to the potential evapotranspiration of 1 m yr^{-1} in the field area (Chiew et al., 2002), shows that even saturated soils will return to near-original reflectance in significantly less than one day. This time is short compared to the compositing time of the MODIS data, effectively minimizing the impact of wetting events on reflectance. Even if soil moisture variability were to have a significant effect on the variability of the soil spectrum in MODIS images, at the coarse spectral resolution of MODIS the main impact of wetting is to reduce the total reflectance rather than significantly change the shape of the soil spectrum. Besides changes in soil surface moisture, other changes to the soil that would cause a considerable change in soil reflectance either occur over very long times compared to the period of this research (i.e., weathering,

oxidation, growth of a biological crust, winnowing, or development of a lag gravel) or occur over very small areas compared to the size of a MODIS pixel (i.e. development of a trail, track, or road from foot or vehicular traffic).

The spectrum of vegetation in RSMA can change through time, but is modeled at all times as a linear combination of invariant GV and NPV spectra, always chosen (as in, Okin, 2007) to be very green (full canopy of green grass) and very brown (full canopy of dry/senescent grass) spectral endmembers. Although there is a considerable amount of variation in vegetation spectra, the shape of the very "green" and very "brown" examples have a remarkable degree of consistency, particularly in coarse resolution remotely sensed data, such as MODIS (e.g., Fig. 2, Asner and Heidebrecht, 2005). Thus, the assumption of invariant GV and NPV spectra used in RSMA as endmembers for the modeling of pixel-wide vegetation at any phase of greenness/brownness is a strong assumption that allows RSMA to elicit temporally and spatially consistent timeseries of GV, NPV, and soil dynamics (Okin, 2010). This is particularly the case here, where the crop species on the target fields (cereal crops, legumes and rapeseed/canola) exhibit typical green and brown spectra during their growing and senescent phases, respectively (e.g., Fig. 2, Nagler et al., 2000, 2003; Nidamanuri and Zbell, 2011). Thus, the original RSMA spectra (Okin, 2007) are not only very close to those found in the field area, but their use allows us to maintain consistency with earlier applications of RSMA.

In RSMA, the apparent surface reflectance of a pixel at time t_i, is modeled as:

$$\rho_{\text{pixel}}^{t_i} = x_{\text{GV}}^{t_i}\rho_{\text{GV}} + x_{\text{NPV}}^{t_i}\rho_{\text{NGV}} + x_{\text{B}}^{t_i}\rho_{\text{B}} + \varepsilon, \tag{5}$$

where,

$$x_{\text{GV}}^{t_i} + x_{\text{NPV}}^{t_i} + x_{\text{B}}^{t_i} = 1. \tag{6}$$

The terms x_{B}, x_{GV}, and x_{NPV} replace the more familiar fractional area terms (denoted as f in Eq. 1) in SMA. x_{GV}, x_{NPV}, and x_{B} are hereafter called RSMA "indices" because they provide an index of the change of these groundcover components from the reference time without providing actual fractional cover values. Values of x_{GV} and x_{NPV} can be positive or negative. x_{B} can be shown to be the ratio of the non-vegetation (interpreted as soil) fractional cover at time t_i to the non-vegetation fractional cover at time t_o, and therefore varies around one rather than zero, like x_{GV}, x_{NPV}. Values of x_{GV}, x_{NPV}, and x_{B} are the best-fit coefficients for Eq. (5) that minimize the RMSE_{S} calculated using Eq. (3). The GV and NPV spectra originally published in Okin (2007) were used here (Fig. 2). Unmixing was conducted using the "la_least_square_equality" routine in IDL (Excelis Visual Information Solutions, Inc., Boulder, Colorado; Anderson et al., 1999), which minimizes squared error and forces the coefficients to sum to one. The advantage to this approach compared to another linear unmixing method using linear algebraic least-squares analysis (including a QR decomposition using the Gram–Schmidt process or the use of singular value decomposition (SVD)) is that constraints can be strictly enforced; in particular, the sum of fractions can be forced to equal exactly one. In cases where there exists a solution for the endmembers that falls within the constraints, both the method used here and a linear algebraic least-squares will provide the same solution.

2.4.4. Calibration of RSMA to absolute cover values

RSMA index values are related to the *difference* between the cover of a ground cover component at time t_i and the cover of a ground cover component at t_o, the reference time (Okin, 2007). RSMA index values, as differences, should therefore be directly relatable to the difference in the measured cover between time t_i and t_o. This logic provides a means to calibrate RSMA index values to absolute cover estimates, with:

$$Y_j^{t_i} = x_j^{t_i}M_j + B_j + f_j^{t_o}, \tag{7}$$

where $Y_j^{t_i}$ is the array of empirically corrected RSMA indices of ground component, j (GV, NPV, or soil). Values of $Y_j^{t_i}$ can be interpreted as estimates of absolute cover at some time ($t_i \neq t_o$, sensu Eqs. 4 and 5). $x_j^{t_i}$ is the array of original RSMA index values at t_i of ground component j. $f_j^{t_o}$ is the array of in situ fractional cover estimates of ground component j at the reference time, t_o. M_j and B_j are the slope and intercept for ground cover component j of the least-squares linear regression:

$$\left(f_j^{t_i} - f_j^{t_o}\right) = M_j x_j^{t_i} + B_j + \varepsilon, \tag{8}$$

where $f_j^{t_i}$ is the array of in situ fractional cover estimates at time t_i, and ε is the fitting error.

In practice, to avoid the use of training data in estimation of the cover estimated provided by this method, a leave-one-out approach was used. The procedure given in Eqs. (7) and (8) was used nine times. Each time, data from a different field were left out of the calculations. The mean and standard deviation of the slopes, intercepts, and correlations (i.e., $\sqrt{R^2}$) were reported. RMSE was calculated using actual fractional cover values and predicted fractional cover values from the omitted fields.

2.4.5. Comparison with in situ data

To determine the degree to which remote sensing indices or estimated cover values agree numerically with in situ data, we calculated linear regression relationships between remotely-sensed values and in situ values. In this analysis, remotely-sensed values were treated as the independent variable and in situ values were treated as the dependent variable. Errors in remote sensing estimates of fractional cover were calculated using two metrics, RMSE_{C} and mean absolute error (MAE_{C}):

$$\text{RMSE}_{\text{C}} = \left(\frac{1}{n}\sum_{i=1}^{n}\left(f_j^{t_i}(i,\text{rs}) - f_j^{t_i}(i,\text{in situ})\right)^2\right)^{1/2}, \tag{9}$$

and

$$\text{MAE}_{\text{C}} = \left(\frac{1}{n}\sum_{i=1}^{n}\left(f_j^{t_i}(i,\text{rs}) - f_j^{t_i}(i,\text{in situ})\right)\right), \tag{10}$$

where n is the number of fields (9) times the number of dates for which cover was estimated (3), $f_j^{t_i}(i,\text{insitu})$ is the in situ estimate of fractional cover for the jth endmember at time t_i for the ith field-date combination, $f_j^{t_i}(i,\text{rs})$ is the remote sensing estimate of fractional cover for the jth endmember at time t_i for the ith field-date combination, and the subscript 'C' refers to the error in fractional cover (to differentiate from the spectral fitting error in Eq. 3).

For the pooled regression and error analysis, the RSMA index x_{B}, which naturally varies around one, was replaced by x_{B}-1 so that it would vary around zero as the others do.

3. Results

In situ estimates of f_{GV}, f_{NPV} and f_{Soil} followed the expected temporal patterns (Table 2). In April (mid-Autumn), fields were dominated by crop residues resulting in high f_{NPV}, while summer weeds provided some f_{GV}. In some fields, low crop-residue retention or extensive utilization of crop residues lead to high f_{Soil}. In June (winter), all fields had been cultivated and crop germination resulted in a mixture of low to moderate f_{GV}, f_{NPV} and f_{Soil}. The October survey was timed to coincide with the expected period of maximum green crop canopy

Table 2
Estimated in situ fractional cover.

	Field	f_{GV}	f_{NPV}	f_{Soil}
April 27, 2010	1	0.08	0.60	0.32
	2	0.05	0.63	0.31
	3	0.07	0.65	0.29
	4	0.15	0.52	0.33
	5	0.20	0.50	0.29
	6	0.10	0.65	0.25
	7	0.12	0.58	0.30
	8	0.00	0.66	0.34
	9	0.04	0.70	0.26
July 22, 2010	1	0.16	0.56	0.28
	2	0.40	0.41	0.18
	3	0.27	0.43	0.30
	4	0.16	0.61	0.24
	5	0.34	0.26	0.39
	6	0.39	0.30	0.32
	7	0.23	0.43	0.34
	8	0.39	0.43	0.19
	9	0.23	0.49	0.27
October 8, 2010	1	0.98	0.01	0.01
	2	0.89	0.11	0.00
	3	0.76	0.12	0.12
	4	0.98	0.01	0.01
	5	0.90	0.05	0.04
	6	0.83	0.08	0.09
	7	0.93	0.06	0.01
	8	0.99	0.01	0.00
	9	1.00	0.00	0.00

density and recorded universally high f_{GV}. The average fraction of shade from photographs in the October survey was 2%.

On average, MESMA fit the MODIS reflectance spectra with $RMSE_S = 2\%$ (reflectance units), better than SMA ($RMSE_S = 3\%$) and RSMA ($RMSE_S = 6\%$). Since normalization was conducted after unmixing, the $RMSE_S$ of the normalized SMA and MESMA fractions must be calculated post hoc. To do this, MODIS reflectance can be predicted using the normalized SMA and MESMA fractions and then using this prediction to estimate $RMSE_S$. This procedure results in $RMSE_S = 15\%$ for normalized SMA and $RMSE_S = 10\%$ for normalized MESMA.

To determine the extent to which remote sensing indices or estimated cover values agree with each other, regardless of in situ data, we calculated correlation coefficients among the different techniques (Tables 3 and 4). All correlations were statistically significant ($\alpha = 0.01$, $n = 26$, $r_{crit} = 0.496$ Rohlf and Sokal, 1981) at ≥ 0.99, ≥ 0.91, and ≥ 0.73 for GV, NPV, and soil, respectively. The worst correlations were for soil cover between MESMA (both normalized and non-normalized) and RSMA (both $r \geq 0.73$). MESMA (both normalized and non-normalized) also shows some disagreement with SMA (both normalized and non-normalized) with r between 0.80 and 0.85. A pooled analysis looking simultaneously at all ground components (i.e., bottom quadrant in Table 3) also shows a significant correlation ($r \geq 0.91$) for all methods. This analysis could not be conducted for RSMA. Since the RSMA index values can be either positive or negative, depending on whether the fractional coverage has increased or decreased since the reference time, whereas fractional cover values from the other remote sensing methods will always be positive, pooled correlation between RSMA indices and other methods does not provide any information about the relative performance of RSMA with other methods and was not calculated.

For methods that directly provide estimates of absolute fractional cover of ground components (SMA, normalized SMA, MESMA, and normalized MESMA), root mean squared difference (RMSD, calculated in the same fashion as Eq. 9) and mean absolute difference (MAD, calculated in the same fashion as in Eq. 10) were calculated between all methods (Tables 3 and 4). Here, "difference" replaces "error" because neither of the methods is privileged. EVI and RSMA, because they provide only indices, cannot be used to calculate RMSD or MAD with other indices or estimates of cover. RMSD provides information about how different the estimates were, whereas MAD provides information on the bias in the estimates. For simplicity, only the sign of MAD is reported. For GV, RMSD shows that SMA and MESMA provided nearly the same estimates (RMSD = 0.01) and normalized SMA and normalized MESMA provided nearly the same estimates (RMSD = 0.05). RMSD is 0.24–0.25 when normalized and non-normalized methods are compared. For NPV, MESMA and normalized SMA provide the closest estimates (RMSD = 0.06) while SMA and MESMA provide the next closest (RMSD = 0.11) and the other comparisons yield RMSD > 0.14. For soil, the closest estimates are provided by SMA and MESMA (RMSD = 0.08) and normalized MESMA and MESMA provide the next closest estimates (RMSD = 0.12). For the pooled comparison, the closest estimates are provided by SMA and MESMA (RMSD = 0.08)

Table 3
Relationship among remote sensing indices or estimated cover values of GV (top quadrant) and for all cover types (pooled, bottom quadrant). Entries with only one number display the correlations between the indices that do not give absolute estimates of cover (EVI and RSMA) and other methods. For other entries, the symbol in parentheses is the sign of the mean absolute difference between the cover values, the first number is the root mean squared difference (RMSD) between cover values, and the second number is the correlation (r) between cover values. Mean absolute difference (MAD) is calculated as the cover value for the method in the column minus the cover value for the method in the row.

	EVI	RSMA	SMA	Norm SMA	MESMA	Norm MESMA
EVI	n/a	0.99	1.00	0.99	1.00	0.99
RSMA	n/a	n/a	1.00	1.00	1.00	1.00
SMA	n/a	n/a	n/a	(−) 0.25, 1.00	(−) 0.01, 1.00	(−) 0.24, 1.00
Norm SMA	n/a	n/a	(+) 0.20, 0.99	n/a	(+) 0.25, 0.99	(+) 0.05, 1.00
MESMA	n/a	n/a	(+) 0.08, 0.91	(−) 0.20, 0.92	n/a	(−) 0.24, 1.00
Norm MESMA	n/a	n/a	(+) 0.23, 0.92	(+) 0.12, 0.93	(+) 0.18, 0.99	n/a

Table 4
Relationship among remote sensing indices or estimated cover values of NPV (bottom quadrant) and soil (top quadrant). Entries with only one number display the correlations between the indices that do not give absolute estimates of cover (RSMA) and other methods. For other entries, the symbol in parentheses is the sign of the mean absolute difference between the cover values, the first number is the root mean squared difference (RMSD) between cover values, and the second number is the correlation (r) between cover values. Mean absolute difference (MAD) is calculated as the cover value for the method in the column minus the cover value for the method in the row.

	RSMA	SMA	Norm SMA	MESMA	Norm MESMA
RSMA	n/a	0.92	0.94	0.73	0.73
SMA	0.92	n/a	(−) 0.19, 0.99	(+) 0.08, 0.81	(−) 0.15, 0.80
Norm SMA	0.91	(+) 0.14, 0.99	n/a	(+) 0.22, 0.85	(+) 0.15, 0.85
MESMA	0.92	(+) 0.11, 0.97	(−) 0.06, 0.96	n/a	(−) 0.12, 0.99
Norm MESMA	0.91	(+) 0.28, 0.98	(+) 0.14, 0.98	(+) 0.17, 0.99	n/a

and normalized SMA and MESMA provide the next closest estimates (RMSD = 0.12).

MAD indicates for all cover types (and the pooled analysis) that normalized SMA and MESMA cover estimates are greater than their non-normalized counterparts (Tables 3 and 4). This result is the direct consequence of the normalization process, where fractional cover values are multiplied by a factor ≥ 1.

Remotely-sensed indices of GV, NPV, and soil (EVI is an index of GV cover, RSMA provides indices of GV, NPV, and soil) and estimates of fractional cover of these ground cover components (SMA and MESMA) followed very similar temporal patterns as in situ estimates (Fig. 3). Plots of index/cover values vs. in situ data (Fig. 4) show strong linear relations between remote sensing methods and in situ data.

The relationship between RSMA indices and in situ fractional cover should be linear, and for this reason, the correlation between RSMA indices and in situ data is the correct basis of comparison. On this basis, the RSMA soil index actually has the highest correlation with soil cover of all methods (0.92, Table 5). Other correlations between remotely-sensed and in situ ground cover component estimates were best for GV ($r \geq 0.94$), compared to NPV ($r \geq 0.89$) and soil ($r \geq 0.84$) (Table 5), and all correlations between remotely-sensed and in situ estimates were significant ($\alpha = 0.01$, n = 26, rcrit = 0.496 Rohlf and Sokal, 1981). A pooled analysis looking simultaneously at all ground components (i.e., "Pooled" in Table 5) also shows a significant correlation ($r \geq 0.78$) for all methods. The relatively low pooled correlation for RSMA results from the fact that RSMA index values can be either positive or negative, depending on whether the fractional coverage has increased or decreased since the reference time, whereas fractional cover values from the other remote sensing methods will always be positive. Therefore, pooling all of the cover types results in the superposition of lines that do not, and should not, all have the same intercept. For example, the fields during the time of reference image (DOY 113, 2010; April 27, 2010) had the lowest f_{GV} and the highest f_{NPV} compared to the other two dates. Therefore $x_{GV}^{t_i}$ will be positive for the other two dates (i.e., higher than the reference time) and $x_{NPV}^{t_i}$ will be negative for the other two dates. In contrast, $f_{GV}^{t_i}$ and $f_{NPV}^{t_i}$ are always positive. Thus, even though the $x_{GV}^{t_i}$ vs. $f_{GV}^{t_i}$ and $x_{NPV}^{t_i}$ vs. $f_{NPV}^{t_i}$ relationships have

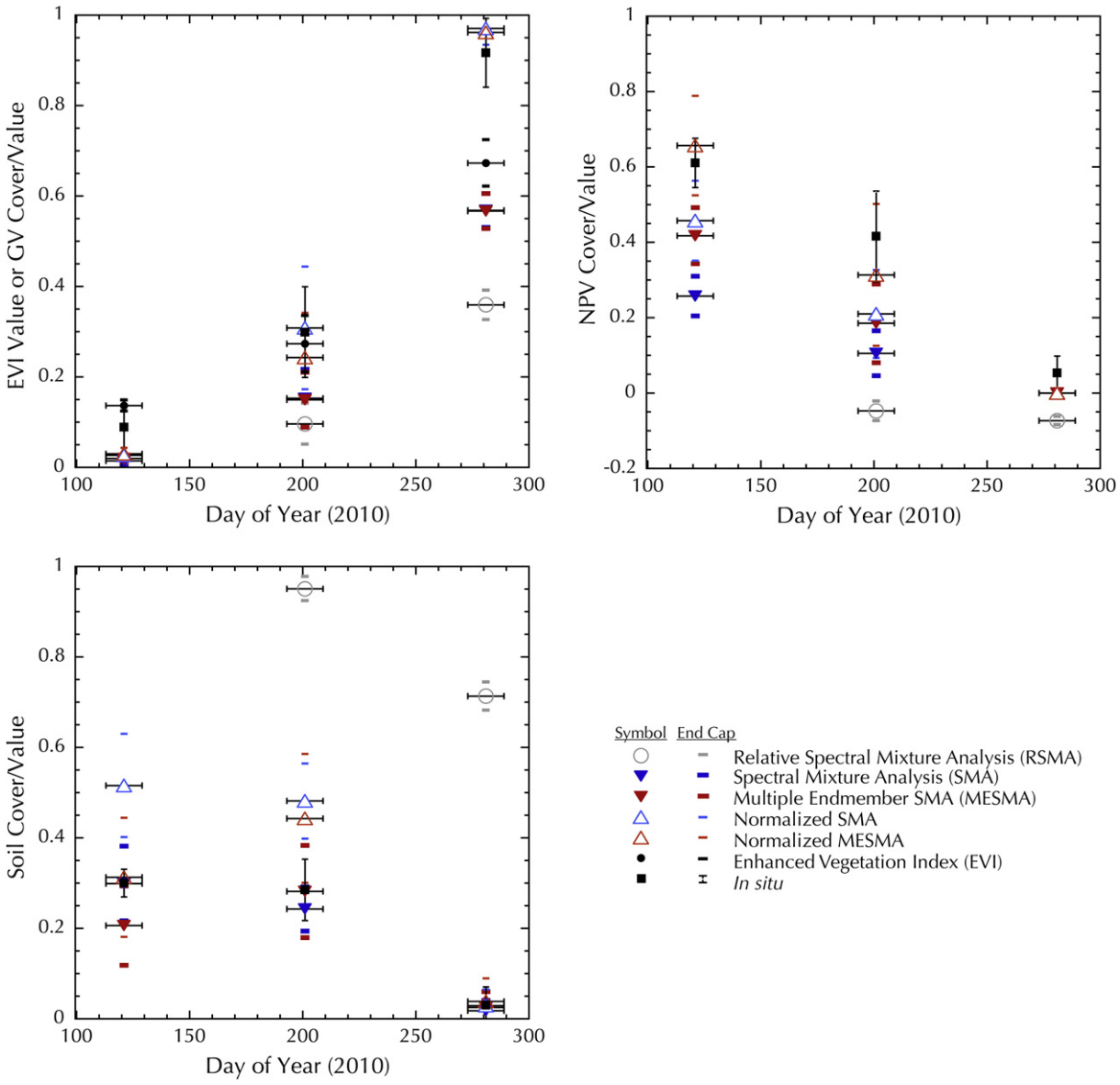

Fig. 3. Time series of average values for all fields of in situ and remotely-sensed index/cover values for GV, NPV, and soil. Horizontal bars represent the compositing time for each remotely-sensed value. End cap symbols depict the ends of vertical bars representing the standard deviation of index/cover values for all fields on each date.

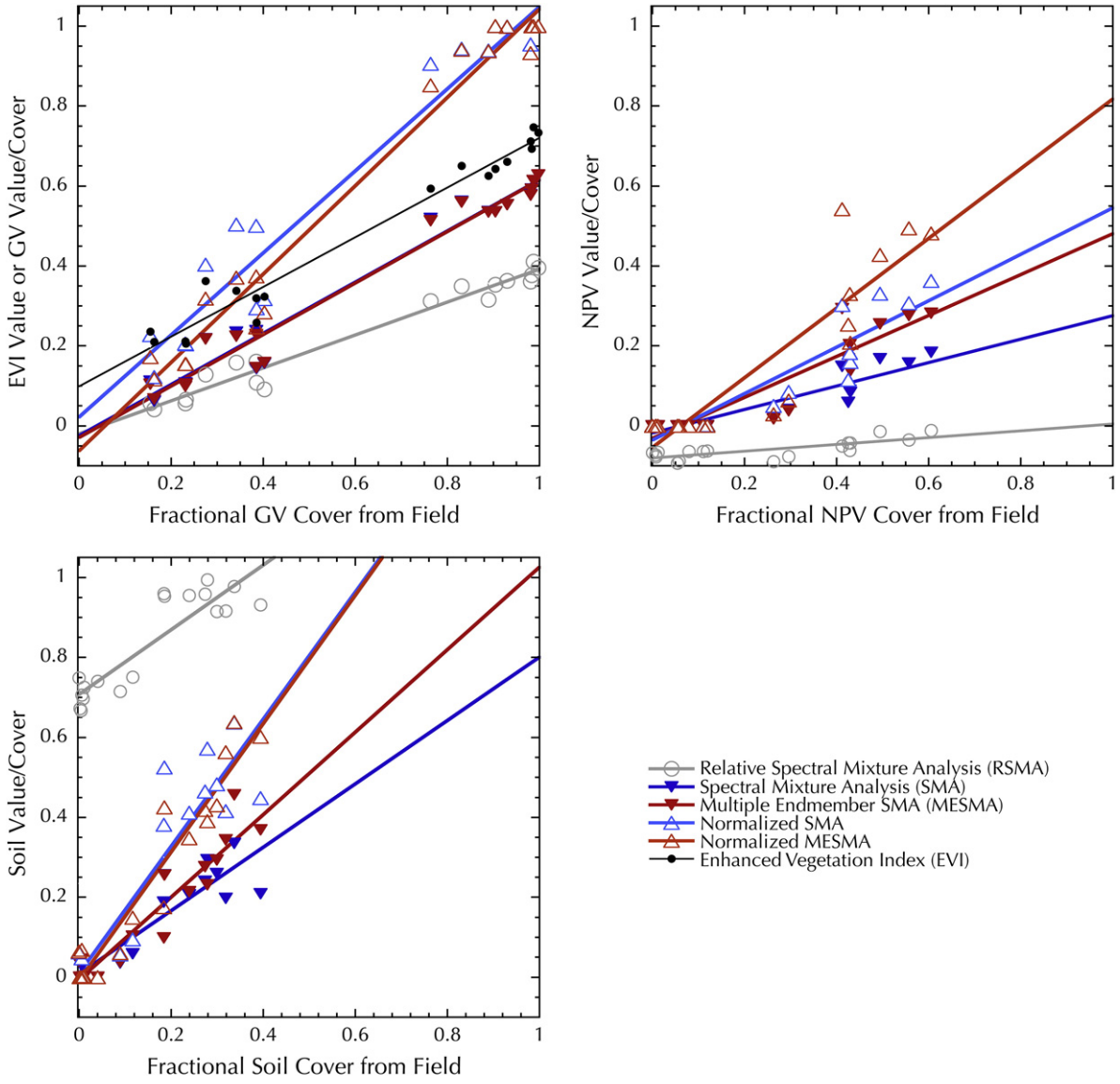

Fig. 4. Remotely-sensed index/cover values for GV, NPV, and soil plotted against in situ values. Lines are best-fit linear regressions.

high correlations, the correlation when the GV and NPV points are considered together must be lower because the intercepts for GV and NPV are different.

For RSMA, a slightly different correlation analysis was also examined. Because RSMA is a relative index, the average correlation for all fields between RSMA timeseries and in situ fractional cover estimates

Table 5
Correlation and regression analysis of remote sensing results against in situ data.

	GV			NPV			Soil			Pooled		
	r	m	*b*	*r*	*m*	*b*	*r*	*m*	*b*	*r*	*m*	*b*
EVI	0.99	1.54	−0.13	–	–	–	–	–	–	–	–	–
RSMA	0.99	2.31	0.08	0.89	6.42	0.62	0.92	0.95	−0.64	0.78	1.35	0.33
SMA	0.99	1.50	0.06	0.92	1.97	0.13	0.87	0.86	0.04	0.86	1.36	0.08
Normalized SMA	0.98	0.88	0.05	0.92	1.10	0.12	0.90	0.50	0.03	0.86	0.79	0.07
MESMA	0.99	1.51	0.06	0.93	1.24	0.12	0.84	0.83	0.06	0.94	0.83	0.06
Normalized MESMA	0.99	0.89	0.07	0.93	0.77	0.12	0.84	0.55	0.06	0.93	1.36	0.05
Calibrated RSMA[a]	0.94	0.94	0.03	0.66	0.66	0.08	0.83	0.83	0.03	0.93	0.93	0.03
Δ(EVI)	0.97	1.57	−0.02	–	–	–	–	–	–	–	–	–
Δ(RSMA)	0.96	2.35	−0.02	0.68	6.43	0.02	0.84	0.99	0.02	0.85	1.91	0.00
Δ(SMA)	0.96	1.50	−0.01	0.77	2.15	0.07	0.63	0.62	−0.04	0.94	1.42	0.01
Δ(Normalized SMA)	0.94	0.91	−0.05	0.79	1.16	0.04	0.74	0.40	−0.04	0.94	0.83	0.00
Δ(MESMA)	0.96	1.50	0.01	0.85	1.43	0.10	0.80	0.67	−0.11	0.95	1.31	0.02
Δ(Normalized MESMA)	0.96	0.87	0.01	0.81	0.78	0.02	0.83	0.46	−0.11	0.96	0.81	0.00

[a] *r*, *m*, and *b* calculated here with omitted data from leave-one-out procedure.

Table 6
Error metrics of remote sensing fractional cover results compared against in situ data.

	GV		NPV		Soil		Pooled	
	MAE_C	$RMSE_C$	MAE_C	$RMSE_C$	MAE_C	$RMSE_C$	MAE_C	$RMSE_C$
EVI	–	–	–	–	–	–	–	–
RSMA	–	–	–	–	–	–	–	–
SMA	−0.19	0.23	−0.24	0.29	−0.02	0.07	−0.15	0.21
Normalized SMA	0.00	0.08	−0.14	0.17	0.14	0.19	0.00	0.16
MESMA	−0.19	0.23	−0.16	0.19	−0.03	0.08	−0.13	0.11
Normalized MESMA	−0.02	0.07	−0.04	0.12	0.06	0.13	0.00	0.18
Calibrated RSMA[a]	0.00	0.10	0.00	0.18	0.00	0.09	0.00	0.13
Δ(EVI)	–	–	–	–	–	–	–	–
Δ(RSMA)	–	–	–	–	–	–	–	–
Δ(SMA)	−0.17	0.22	0.16	0.23	−0.02	0.13	−0.01	0.20
Δ(Normalized SMA)	0.10	0.15	0.02	0.14	−0.12	0.22	0.00	0.17
Δ(MESMA)	−0.17	0.22	0.04	0.13	0.09	0.14	−0.01	0.17
Δ(Normalized MESMA)	0.06	0.12	−0.13	0.19	0.07	0.18	0.00	0.17

[a] r, m, and b calculated here with omitted data from leave-one-out procedure.

is instructive (n = 3 for these correlations for the three dates at which the fields were measured). These values are not amenable to statistical test, but are nonetheless high: 0.99, 0.93 and 0.94 for GV, NPV, and soil, respectively. This same method could have been used for other remote sensing cover estimates, but is not necessary since other methods aren't relative but absolute.

Normalized SMA and normalized MESMA had regression slopes closest to one for GV and NPV excluding residual-corrected RSMA (which is forced to have slopes and intercepts of regression of one and zero, respectively) (Table 5). When considering the slope of the relationship for soil, simple (i.e. non-normalized) SMA and MESMA outperformed their normalized counterparts (i.e., had slopes closer to one). This pattern is also reflected in $RMSE_C$ (Table 6). Normalized SMA and normalized MESMA had the lowest $RMSE_C$ for GV (0.08 and 0.07, respectively). For NPV, $RMSE_C$ was higher, though normalized SMA and normalized MESMA had the lowest $RMSE_C$ (0.17 and 0.12, respectively). Non-normalized SMA and MESMA outperformed their counterparts in terms of $RMSE_C$ of soil cover (0.07 and 0.08).

SMA and MESMA exhibited negative values of MAE_C for all cover types (Table 6), indicating that predicted fractional cover was on average lower than in situ fractional cover. This is true for all dates (not shown). For GV, normalized SMA predictions were unbiased and MAE_C was only slightly negative for normalized MESMA. For NPV, normalized SMA and MESMA resulted in negative values of MAE_C but positive values of MAE_C were observed for normalized SMA and MESMA soil fractions. In the pooled data, the positive and negative biases for normalized SMA and MESMA cases canceled each other out, resulting in no net bias.

Calibration of RSMA data to fractional cover using the procedure discussed above (i.e., a leave-one-out implementation of Eqs. 7 and 8) was conducted. For GV and NPV, correlations between calibrated RSMA values and actual cover values were lower than all other methods (Table 5). For soil, the correlation coefficient was equal to the minimum for all other methods. Variation in slope and intercept estimates for GV and soil was very small (Table 6), and it was slightly greater for NPV, reflecting the higher variance (and lower correlation) seen with this ground component. For the pooled analysis of all fractional cover, calibrated RSMA had the second highest (0.93 vs. 0.94 for MESMA) correlation, the slope closest to one (0.93) and the lowest intercept (0.03). This procedure resulted in unbiased (i.e., $MAE_C = 0$) estimates of fractional cover. $RMSE_C$ values of calibrated RSMA were comparable to those from other methods, with values intermediate to the values from other methods. That is to say, the calibrated RSMA in some cases performed better than SMA and MESMA, and sometimes worse. In the pooled case, the $RMSE_C$ value for calibrated RSMA was second lowest (0.13 vs. 0.11 for MESMA).

A unique aspect of our in situ data is that they were acquired over three different dates. The MODIS data are multitemporal as well. This allows an analysis not only of the absolute index values and fractions, but also of their change. For RSMA and calibrated RSMA, these comparisons are one and the same because RSMA provides information on the changes in fraction from the reference time. For GV, correlation between Δ(EVI) and $\Delta(f_{GV})$ was the highest (0.97) and that between Δ(normalized SMA) and $\Delta(f_{GV})$ was the lowest (0.94) with all others being equal (0.96) (Table 5, bottom). For NPV, Δ(RSMA) had the lowest correlation with $\Delta(f_{NPV})$, whereas Δ(MESMA) had the highest correlation with $\Delta(f_{NPV})$. For soil, Δ(RSMA) had the highest correlation with $\Delta(f_{NPV})$, whereas Δ(SMA) had the lowest correlation with $\Delta(f_{NPV})$. For the pooled analysis Δ(normalized MESMA) exhibited the best correlation with changes in field fractional cover, whereas Δ(RSMA) exhibited the lowest correlation. Of all relationships, only the $\Delta(f_{Soil})$ vs Δ(RSMA) comparison yielded a relationship that fell very near the 1:1 line (m = 0.99, b = 0.02), with the $\Delta(f_{GV})$ vs. Δ(normalized SMA) exhibiting a slope near one, but with considerable overprediction (MAE_C = 0.10, consistent with $m<1$ and $b<0$ for the $\Delta(f_{GV})$ vs. Δ(normalized SMA) line).

For GV, the smallest bias (MAE_C) and lowest error ($RMSE_C$) was observed for Δ(normalized MESMA), whereas Δ(MESMA) had the lowest error for NPV and soil (Table 6, bottom). Δ(normalized MESMA) exhibited the least biased estimates of $\Delta(f_{NPV})$ and Δ(SMA) exhibited the least biased estimates of $\Delta(f_{Soil})$. Overall, biases for all methods were low (MAE_C = −0.01–0.0) and errors were nearly equal ($RMSE_C$ = 0.17 for all except Δ(SMA) with $RSMA_C$ = 0.20).

4. Discussion

In this study, we compared several methods for use with MODIS NBAR data that can be used either to produce indices of change in GV, NPV and soil (EVI, RSMA) or to produce absolute estimates of these ground cover components. Our results did not indicate that a single technique worked best in all circumstances, particularly when bias (MAE_C) and absolute error ($RMSE_C$) were considered.

Comparisons among remote sensing methods (Tables 3 and 4) are informative. The information content of the remote sensing imagery used to produce indices or fractional cover estimates of GV, NPV, and soil is the same because the imagery is all the same. In the case of RSMA, SMA, and MESMA, the same NBAR data was used as input in our calculations. EVI is also produced from this NBAR data, though we downloaded the MODIS product rather than calculating it ourselves. Given the same input data, then, comparisons among results from different methods provide information on the inherent differences among the analytical methods, regardless of in situ data. The

results in Tables 3 and 4 therefore provide benchmarks against which comparisons with in situ data can be made. In situ data carry their own estimation errors and biases and it is unreasonable to expect that comparisons with in situ data yield better relationships than comparisons among remote sensing techniques; since they use the same input data (i.e., imagery), imagery-related errors and bias are consistent among remote sensing methods.

The source of disagreement (i.e., high RMSD despite high correlation) between normalized and non-normalized versions of SMA and MESMA are clear; normalization systematically changes fractional cover estimates so even if SMA and MESMA provide the same estimates of fractional cover (i.e., low RMSD), normalization will increases RMSD when comparing normalized and non-normalized versions of the same technique. This effect is visible in all cover types as well as the pooled data (Table 3). In the pooled data, for instance, the lowest RMSDs are 0.08 and 0.12, respectively, for the SMA–MESMA and normalized SMA–normalized SMA comparison (i.e., apples-to-apples comparisons vis a vis normalization). Thus, if the values of RMSD are used as a benchmark for the pooled data, we would not expect $RMSE_C$ values to be lower than 0.08–0.12. Indeed, the lowest $RMSE_C$ is 0.11 (for MESMA), which is comparable to the lowest RMSDs (0.08–0.12).

For pooled data, this suggests that $RMSE_C$ is as low as can be expected, suggesting that MESMA is giving the best possible pooled estimates of cover. The situation is somewhat different when examining individual cover types. For GV, the lowest $RMSE_C$ is seven times the value of the lowest RMSD (0.07 vs. 0.01), suggesting that even though GV estimates are better than the other cover types, they are far from what they could be optimally. On the other hand, the lowest $RMSE_C$ for soil is approximately equal to the lowest RMSD ($RMSE_C$ = 0.07 for SMA vs. RMSD = 0.08) suggesting that soil retrievals for SMA are as good as they are likely to get, at least using the set of endmembers employed here.

Comparisons between RSMA indices and SMA or MESMA results cannot, unfortunately, use RMSD because these techniques provide different types of values. For NPV, though, we see that RSMA index values and fractional cover from the SMA techniques are highly correlated (Table 4). It is therefore unsurprising that the correlations for all of these techniques with MESMA data are about the same (r = 0.89–0.93). The soil results tell a different story, however. RSMA soil index values and SMA fractional cover values are highly correlated (r = 0.92–0.94), but the correlation between RSMA and MESMA fractional cover values display a much lower correlation (r = 0.73) (Table 4). Indeed, the SMA and MESMA correlation is also low (r = 0.81) indicating some difference between RSMA/SMA and MESMA. Since the input imagery is the same in all cases, the difference must be inherent to the techniques themselves. Since the same code was used to calculate fractions from SMA and MESMA the only possible difference between these techniques is the availability of additional endmembers in MESMA. However, we see that the consequence of the availability of additional endmembers is not to improve the correlation with in situ soil fractional cover estimates, because correlation coefficients are actually higher (and $RMSE_C$ is lower) for SMA compared to MESMA. It cannot be assumed that MESMA always makes soil fractional cover estimates better. Okin et al. (2001) showed that "coupling" between soil and NPV spectra can actually lead to error in MESMA as some combinations of soil/NPV can masquerade as combinations of other soil/NPV. This question can only be answered by comparing with in situ estimates, to which we now turn.

There are features of Figs. 3 and 4, which display comparisons between remote sensing and in situ results, that might lead to misleading interpretations of the RSMA results. RSMA, unlike the other methods, provides an index of change relative to some reference time. If, for example, the fractional cover of NPV is 0.5 at the reference time and also at a later date, the RSMA NPV index will be zero at that later date despite the non-zero fractional cover of NPV. Therefore, in a plot against absolute fractional cover from in situ measurements (as in Fig. 4), the 1:1 line has no special meaning for the RSMA indices. Furthermore, the RSMA soil index, x_B, varies around one rather than zero, unlike the other RSMA indices. So, while no change in GV and NPV cover from the reference time would give RSMA GV and NPV index values of zero, no change in soil cover would give an RSMA soil index value of one. As a result, values of RSMA index values tend not to cluster with others in Figs. 3 and 4 and this difference is especially glaring for soil.

As an index of GV change our data suggests that x_{GV}, from RSMA, and f_{GV} from SMA and MESMA are as useful as EVI. The benefit of EVI is its computational simplicity and availability of a standard MODIS product. The benefit of SMA and MESMA are the fact that they provide absolute GV cover estimates, though the availability and choice of endmembers complicate these methods. The benefit of RSMA is that it provided strong correlations with in situ GV cover without the need for additional information (i.e., using endmembers that appeared in the original RSMA publication (Okin, 2007)), though it can only provide information about the change of GV cover rather than the absolute fractional cover.

However, the development of RSMA was spurred not by the need for another GV index, but rather by the need for remotely-sensed information about NPV and soil. When correlations among remotely-sensed values of NPV are considered, we see greater disagreement than with GV (i.e., lower correlations). These differences highlight the difficulty of extracting information on NPV from satellite-derived surface reflectance. Nonetheless, the RSMA index of NPV performs well, and essentially equally, when compared to SMA and MESMA (both normalized and non-normalized) (Table 5). Retrieval of NPV from reflectance imagery is made difficult, in part, by the fact that its spectrum can be so similar to that of the soil, particularly in multispectral imagery (Fig. 2 and Okin (2007)). The NPV signal is therefore subtle in the presence of soil background and the lower correlations for NPV compared to GV are a likely consequence.

The only direct comparison possible between RSMA indices and in situ fractional cover is correlation; there is no reason to expect that the magnitude of absolute RSMA should match that of fractional cover, just as the magnitude of EVI should not match that of GV fractional cover. For GV and NPV, the correlations between RSMA indices and in situ fractional cover are high and comparable to those from SMA/MESMA retrieval (0.99 vs. 0.99 and 0.89 vs. 0.92–0.93, respectively; Table 5). For soil, the correlation between RSMA indices (0.92) is greater than that for both normalized and non-normalized SMA and MESMA (0.84–0.90). These results indicate clearly that RSMA provides information on GV, NPV and soil dynamics similar to those provided by the more traditional SMA methods.

A surprising result, despite the simplicity of the RSMA approach and the fact that this method does not utilize a "soil" spectrum in unmixing, is that this method provides excellent predictions (with slopes close to 1) of changes in soil cover. Indeed, of all methods and all cover types, RSMA provides the best prediction of soil cover change (Table 5).

RSMA was created to provide an index of change of fractional cover ground components, particularly in cases when the spectrum of the soil background is not known. SMA and MESMA, in comparison, require knowledge of the soil spectrum and, in the case of MESMA, several soil spectra to choose from. Indeed, in the results here, we probably inflated the accuracy of SMA by using for SMA the spectra that most often modeled our study area using MESMA. The choice of other spectra for SMA would have changed the accuracy of this approach, but the extent to which alternate endmember selection improves or degrades accuracy would depend, of course, on the endmembers actually used.

Comparing SMA and MESMA it is interesting to note that normalization did not uniformly improve (or degrade) the relationship with field data, particularly when looking at $RMSE_C$. In some cases

where normalization decreased (increased) $RMSE_C$, it also decreased (increased) the correlation coefficient. For GV, normalization of SMA decreased $RMSE_C$ but also slightly reduced the correlation with in situ data. For NPV, normalization did not change the correlation coefficient despite lowering $RMSE_C$. For soil, normalization increased $RMSE_C$ while also increasing the correlation coefficient.

This pattern can be explained by analysis of the values of MAE_C. SMA tends to underestimate ($MAE_C<0$) GV and NPV cover significantly. Soil is only slightly underestimated. This suggests that either 1) the endmembers used in SMA and MESMA were brighter than the effective spectra of these ground cover components in the MODIS scenes such that lower fractions of brighter spectra offset one another, or 2) shade makes up a significant portion of the scene resulting in reduced MODIS-observed reflectance.

Shading of soil by plants would reduce soil fraction and increase GV and NPV fraction (when all endmembers are divided by the sum of non-shade endmembers, as done here). This would thus tend to make negative biases of soil fraction less negative and negative biases of GV and NPV more negative. This might explain, in part, the smaller biases observed for SMA and MESMA soil fractions compared to those of GV and NPV.

Though our point-step methods are not suitable for estimating shade fraction, the photographic method used in the October field survey is, and it results in an estimate of 2% shade. Given relatively high crop cover during the October sampling period compared to the others, it is unlikely that the shade cover during the other periods is much higher than 2%. This is true despite the lower soil zenith angle during the October sampling period: in April, fields were dominated by low crop residue that do not cast much shade and in June, low cover from recently germinated crops also do not cast much shade. This small amount of shade does not seem likely to be able to explain the underestimation of GV and NPV by SMA and MESMA. Thus, a better explanation is that the endmembers used unmixing for these methods are relatively brighter than their in situ counterparts. And indeed, self-shading of plants (resulting in lower apparent reflectance than the reflectance of a single leaf) is a common phenomenon.

By definition, the normalization procedure must increase fractional cover estimates (or, do nothing if fractional covers already sum to one). In the case of GV, this procedure effectively eliminated this bias for GV, lowering $RMSE_C$. Normalization reduced the bias for NPV, thus somewhat lowering $RMSE_C$. For soil, normalization resulted in the opposite bias (i.e., positive MAE_C), increasing $RMSE_C$. Non-normalized estimates of soil fraction using SMA and MESMA were already low, with very small biases. Normalization, in effect, overcompensated for this cover component, throwing off estimates that were already pretty good.

Thus, the fact that non-normalized fractions from SMA and MESMA for soil had lower error than the normalized fractions whereas the opposite is seen with GV and NPV indicates that neither normalization can be prescribed as a best practice. Not normalizing, likewise, cannot be prescribed as a best practice. However, the negative values of MAE_C, indicating underpredictions in the non-normalized case should be considered when evaluating SMA and MESMA fractional cover results.

Calibration of RSMA to yield absolute cover estimates resulted in cover estimates that were comparable to those from other methods, as seen in the $RMSE_C$ (Table 5). The use of the leave-one-out approach here was necessary so as not to use training data in the evaluation of error (i.e. $RMSE_C$). But this practice also allows us to examine the variance in the regression coefficients (i.e., slope and intercept) (Table 7). Low variance of the regression coefficients indicates that, at least in the case examined here, there is significant consistency among the various fields in their respective relationships between RSMA and actual cover. This is likely due to the fact that all fields had similar GV, NPV, and soil cover during the reference time (April 27; Table 2) and, possibly, that the soil reflectance of all of the fields is somewhat similar (Fig. 2). Further research is needed to determine the impact of these two factors (similarity of fractional cover during the reference time and soil spectral characteristics) on RSMA-fractional cover calibrations at other sites and in other circumstances.

Table 7
Estimated slope, intercept, r and $RMSE_C$ for calibration of RSMA indices using a leave-one-out regression approach. Values for slope, intercept, and r are mean (standard deviation). See Eq. (8).

	GV	NPV	Soil
Slope	2.35 (0.04)	6.44 (0.50)	0.99 (0.04)
Intercept	−0.02 (0.01)	0.02 (0.03)	−0.97 (0.03)
r	0.96 (0.00)	0.68 (0.04)	0.84 (0.01)
MAE_C	−0.00084	−0.0045	0.00066
$RMSE_C$	0.10	0.18	0.09

The decrease in correlation coefficient between in situ fractional cover and calibrated RSMA compared to uncalibrated RSMA for all ground cover components is intriguing. All data carry measurement errors, and the estimation of fractional cover of GV, NPV, and soil in the field is especially difficult, particularly when a binary method is used (does a brownish green or greenish brown plant count as GV or NPV?). It is possible, then, that this decrease in correlation coefficient with the addition of field data is due to error in the in situ measurements themselves, or at least variation in the estimated cover that is endemic to the type of field methods used here. Given our approach, there is no guarantee that systematic errors in the field data collection would be accounted for in the regression relationship because the bias/variance on one sampling date may not be the same as the bias/variance on another sampling date. For instance sampling bias/variance can be expected to be very different when the vegetation is entirely green than when it is in between GV and NPV. Even if the human eye were able to determine exactly when a leaf was more green than brown (i.e., spectrally closer to GV than to NPV), the imposition of a binary category (GV vs. NPV) on a fundamentally continuous property (greenness/brownness) will influence the bias/variance depending on state of the vegetation. Nonetheless, in practice this error appears to be not large enough to engender worry, because the $RMSE_C$ of the calibrated RSMA fractions are not too different from the $RMSE_C$ from the other methods and all are statistically significant when compared with in situ data.

Nevertheless, if one were only interested in fractional cover of soil, our results suggest that the calibration of RSMA index values to fractional cover may not be necessary. The slope near one of the RSMA index values for soil when regressed against in situ values (Table 5) indicates that changes in the RSMA soil index and the actual fractional cover of soil occur on nearly on a 1:1 basis. The slope near one and intercept near zero of the $\Delta(\text{RSMA})$ comparison with $\Delta(f_{soil})$ further support this conclusion.

The results of this study show that the RSMA approach, with the clear tradeoff being that it cannot – without calibration – be used to estimate absolute cover fractions, has merit when compared to other remote sensing methods. The fact that RSMA endmembers were taken from laboratory spectra of green and dry/senescent grass, rather than from the field area, and that these endmembers allowed RSMA to perform well compared to methods that required field data underlines the solidity of this approach; "general" GV and NPV spectra used in the RSMA context resulted in indices that were strongly correlated with ground component fractional cover and, when these indices were calibrated, resulted in absolute fractional cover that was as accurate as MESMA.

5. Conclusion

Remote sensing of the Earth's terrestrial surface has become a vital tool in the understanding of the Earth system. The most common use of optical remote sensing has been in the quantification of GV cover. But GV is not the only component of terrestrial environments, and

for some applications, it is not even the most important component. This is particularly true in drylands where plants aren't always green and erosion and/or fire can be a major concern. Other major (non-snow) ground components, namely NPV and soil, have been increasingly identified as worthy of study, but a dearth of remote sensing methods that can accurately quantify their dynamics, in addition to appropriate datasets to calibrate these methods against, has perhaps hindered scientific advancement in this area.

Like all scientific endeavors and perhaps more than most, remote sensing is characterized by a set of trade-offs. A limited number of photons arriving at a sensor require tradeoffs between bandwidth, pixel size, and noise. Orbital mechanics constrain spaceborne platforms requiring tradeoffs between repeat time and swath width. Here, we observe trade-offs in the amount of data that goes into a technique and how well that technique can retrieve information about the ground surface; SMA and MESMA provide better estimates of the changes of GV and NPV than RSMA but at the cost of needing more ancillary spectral information. We observe tradeoffs in whether normalization improves or degrades fractional cover estimates; for GV and NPV it improves estimates, but for soil it does not. We observe tradeoffs in whether SMA or MESMA, with its greater choice of endmember spectra, improves estimates of fractional cover; for GV and NPV it does, but for soil it does not. We observe tradeoffs in how addition of information for the calibration of RSMA affects fractional cover estimates; it reduces the correlation with in situ data, but produces results nearly as accurate as other techniques.

These tradeoffs suggest that care must be taken in the choice of methods and our results indicate that the approach be tailored to the purpose of the study. A study aimed at examining soil cover for the purpose of erosion estimation should utilize a different method than one aimed at examining NPV cover for fuel load estimation. A study that needs actual fractional cover should use different methods than one that only needs to examine changes in fractional cover. Tradeoffs in the methods also suggest that the method chosen depends, to some extent, on the available data (e.g., endmember spectra vs. fractional cover of ground components at a specific time).

To some extent, but perhaps less than expected, our results indicate the utility of additional information in the form of added endmembers for the remote sensing of ground components. One might expect this to be particularly true in the case of soil due to the amount of variability in soil spectra. However, more information can be too much of a good thing; one well-chosen soil endmember in SMA provided better soil cover estimates than a full MESMA approach. RSMA, which requires no soil spectrum, provided the best quantitative estimates of how soil cover changes. Calibration of RSMA, which again requires the addition of information, can produce fractional cover estimates.

This study used only nine sites and three dates in an agricultural area with, admittedly, simple vegetation structure. As a validation exercise, it cannot be said to represent accuracy for all vegetation types and locations. Further study is required for field areas with more complex vegetation structure and more variable soils. Nonetheless, it is the first study that compares multiple methods for the estimation of GV, NPV, and soil dynamics and provides guidance on what level of accuracy might be expected and where biases might exist.

But, in addition, this study shows significant differences among techniques that have the same mathematical basis (SMA, RSMA, and MESMA are all spectral unmixing techniques) and therefore might be thought to produce similar results. Our results indicate important differences in these techniques showing that, perhaps to an unexpected degree, the most appropriate technique depends on which ground component is the focus of study. Our results further suggest diminishing returns with the inclusion of additional spectral endmembers, an observation that runs counter to intuition and that can be tested in other locations.

Acknowledgments

This research was funded by the Australian Research Council Linkage Project grant LP0990019 with financial and in-kind contributions from the South Australian Department for Environment and Natural Resources in Australia and NASA grants NNX10AO96G and NNX10AO97G in the US.

Thanks to the land-holders, Clinton Tiller and Greg Barr, who graciously gave permission for collection of cover data from their properties. Thanks to the University of Adelaide staff, Victoria Marshall, Kelly Arbon, Valerie Lawley, Yuot Alaak and Lydia Cape-Ducluzeau for the many enthusiastic hours of step-point data collection.

References

Anderson, E., Bai, Z., Bischof, C., Blackford, S., Demmel, J., Dongarra, J., et al. (1999). *LAPACK users' guide* (third ed.). Philadelphia, PA: Society for Industrial and Applied Mathematics (SIAM) [3rd Ed.].

Asner, G. P., & Heidebrecht, K. B. (2002). Spectral unmixing of vegetation, soil and dry carbon cover in arid regions: Comparing multispectral and hyperspectral observations. *International Journal of Remote Sensing*, *23*, 3939–3958.

Asner, G. P., & Heidebrecht, K. B. (2005). Desertification alters regional ecosystem–climate interactions. *Global Change Biology*, *11*, 182–194.

Asner, G. P., Wessman, C. A., Bateson, C. A., & Privette, J. L. (2000). Impact of tissue, canopy, and landscape factors on the hyperspectral reflectance variability of arid ecosystems. *Remote Sensing of Environment*, *74*, 69–84.

Ballantine, J. A. C., Okin, G. S., Prentiss, D. E., & Roberts, D. A. (2005). Mapping North African landforms using continental-scale unmixing of MODIS imagery. *Remote Sensing of Environment*, *97*, 470–483.

Balling, R. C., Jr. (1988). The climatic impact of a Sonoran vegetation discontinuity. *Climatic Change*, *13*, 99–109.

Ben-Dor, E., & Banin, A. (1994). Visible and near-infrared (0.4–1.1 mm) analysis of arid and semiarid soils. *Remote Sensing Of Environment*, *48*, 261–274.

Ben-Dor, E., Goldlshleger, N., Benyamini, Y., Agassi, M., & Blumberg, D. G. (2003). The spectral reflectance properties of soil structural crusts in the 1.2- to 2.5-μm spectral region. *Soil Science Society of America Journal*, *67*, 289–299.

Bonfils, L., de Noblet-Ducoure, N., Braconnot, P., & Joussaume, S. (2001). Hot desert albedo and climate change: Mid-Holocene monsoon in North Africa. *Journal of Climate*, *14*, 3724–3737.

Chabrillat, S., Goetz, A. F. H., Krosley, L., & Olsen, H. W. (2002). Use of hyperspectral images in the identification and mapping of expansive clay soils and the role of spatial resolution. *Remote Sensing of Environment*, *82*, 431–445.

Chiew, F., Qang, Q. J., McConachy, F., James, R., Wright, W., & deHoedt, G. (2002). Evapotranspiration maps for Australia. *Hydrology and Water Resources Symposium*. Melbourne, Australia: Institution of Engineers.

Clark, R. N., King, T. V. V., Klejwa, M., Swayze, G. A., & Vergo, N. (1990). High spectral resolution reflectance spectroscopy of minerals. *Journal of Geophysical Research*, *95*, 12,653–12,680.

Curran, P. J. (1989). Remote sensing of foliar chemistry. *Remote Sensing of Environment*, *30*, 271–278.

Dennison, P. E., Halligan, K. Q., & Roberts, D. A. (2004). A comparison of error metrics and constraints for multiple endmember spectral mixture analysis and spectral angle mapper. *Remote Sensing of Environment*, *93*, 359–367.

Elmore, A. J., Asner, G. P., & Hughes, R. F. (2005). Satellite monitoring of vegetation phenology and fire fuel conditions in Hawaiian drylands. *Earth Interactions*, 9.

Evans, R. A., & Love, R. M. (1957). The step-point method of sampling: A practical tool in range research. *Journal of Range Management*, *19*, 208–212.

Franklin, J., Duncan, J., & Turner, D. L. (1993). Reflectance of vegetation and soil in Chihuahuan desert plant communities from ground radiometry using SPOT wavebands. *Remote Sensing of Environment*, *46*, 291–304.

Gerbermann, A. H. (1979). Reflectance of varying mixtures of clay soil and sand. *Photogrammetric Engineering and Remote Sensing*, *45*, 1145–1150.

Guerschman, J. P., Hill, M. J., Renzullo, L. J., Barrett, D. J., Marks, A. S., & Botha, E. J. (2009). Estimating fractional cover of photosynthetic vegetation, non-photosynthetic vegetation and bare soil in the Australian tropical savanna region upscaling the EO-1 Hyperion and MODIS sensors. *Remote Sensing of Environment*, *113*, 928–945.

Hapke, B. (1981). Bidirectional reflectance spectroscopy. 1. Theory. *Journal of Geophysical Research*, *86*, 3039–3054.

Huete, A., Didan, K., Miura, T., Rodriguez, E. P., Gao, X., & Ferreira, L. G. (2002). Overview of the radiometric and biophysical performance of the MODIS vegetation indices. *Remote Sensing of Environment*, *83*, 195–213.

Jia, G. S. J., Epstein, H. E., & Walker, D. A. (2003). Greening of arctic Alaska, 1981–2001. *Geophysical Research Letters*, *30*, 2067.

Karnieli, A., Kidron, G. J., Glaesser, C., & Ben-Dor, E. (1999). Spectral characteristics of cyanobacteria soil crust in semiarid environments. *Remote Sensing of Environment*, *69*, 67–75.

Kleidon, A., Fraedrich, K., & Heimann, M. (2000). A green planet versus a desert world: Estimating the maximum effect of vegetation on the land surface climate. *Climatic Change*, *44*, 471–493.

Lasdon, L. S., & Waren, A. D. (1986). *GRG2 user's guide.* Cleveland, OH: Cleveland State University.

Lobell, D. B., & Asner, G. P. (2002). Moisture effects on soil reflectance. *Soil Science Society of America Journal*, *66*, 722–727.
Lopez, M. V., Gracia, R., & Arrue, J. L. (2000). Effects of reduced tillage on soil surface properties affecting wind erosion in semiarid fallow lands of Central Aragon. *European Journal of Agronomy*, *12*, 191–199.
Lucht, W., Prentice, I. C., Myneni, R. B., Sitch, S., Friedlingstein, P., Cramer, W., et al. (2002). Climatic control of the high-latitude vegetation greening trend and Pinatubo effect. *Science*, *296*, 1687–1689.
Mentis, M. T. (1981). Evaluation of the wheel-point and step-point methods of veld condition assessment. *African Journal of Range and Forage Science*, *16*, 89–94.
Nagler, P. L., Daughtry, C. S. T., & Goward, S. N. (2000). Plant litter and soil reflectance. *Remote Sensing of Environment*, *71*, 207–215.
Nagler, P. L., Inoue, Y., Glenn, E. P., Russ, A. L., & Daughtry, C. S. T. (2003). Cellulose absorption index (CAI) to quantify mixed soil–plant litter scenes. *Remote Sensing of Environment*, *87*, 310–325.
NASA Land Processes Distributed Active Archive Center (LP DAAC) (2001a). MCD43A4. In USGS/Earth Resources Observation and Science (EROS) Center (Ed.), [Sioux City, South Dakota].
NASA Land Processes Distributed Active Archive Center (LP DAAC) (2001b). MOD13A1. In USGS/Earth Resources Observation and Science (EROS) Center (Ed.), [Sioux City, South Dakota].
Nicholson, S. (2000). Land surface processes and Sahel climate. *Reviews of Geophysics*, *38*, 117–139.
Nidamanuri, R. R., & Zbell, B. (2011). Use of field reflectance data for crop mapping using airborne hyperspectral image. *ISPRS Journal of Photogrammetry and Remote Sensing*, *66*, 683–691.
Okin, G. S. (2007). Relative spectral mixture analysis: A multitemporal index of total vegetation cover. *Remote Sensing of Environment*, *106*, 467–479.
Okin, G. S. (2010). The contribution of brown vegetation to vegetation dynamics. *Ecology*, *91*, 743–755.
Okin, G. S., & Painter, T. H. (2004). Effect of grain size on remotely sensed spectral reflectance of sandy desert surfaces. *Remote Sensing of Environment*, *89*, 272–280.
Okin, G. S., Okin, W. J., Murray, B., & Roberts, D. A. (2001). Practical limits on hyperspectral vegetation discrimination in arid and semiarid environments. *Remote Sensing of Environment*, *77*, 212–225.
Palacios-Orueta, A., & Ustin, S. L. (1998). Remote sensing of soil properties in the Santa Monica Mountains. I. Spectral analysis. *Remote Sensing of Environment*, *65*, 170–183.
Parmesan, C., & Yohe, G. (2003). A globally coherent fingerprint of climate change impacts across natural systems. *Nature*, *421*, 37–42.
Price, J. C. (1990). On the information content of soil reflectance spectra. *Remote Sensing of Environment*, *33*, 113–121.
Reed, B. C. (2006). Trend analysis of time-series phenology of North America derived from satellite data. *Geoscience and Remote Sensing*, *43*, 24–38.
Reed, B. C., Brown, J. F., Vanderzee, D., Loveland, T. R., Merchant, J. W., & Ohlen, D. O. (1994). Measuring phenological variability from satellite imagery. *Journal of Vegetation Science*, *5*, 703–714.
Roberts, D. A., Smith, M. O., & Adams, J. B. (1993). Green vegetation, nonphotosynthetic vegetation, and soils in AVIRIS data. *Remote Sensing of Environment*, *44*, 255–269.
Roberts, D. A., Gardner, M., Church, R., Ustin, S. L., & Green, R. O. (1997). Optimum strategies for mapping vegetation using multiple endmember spectral mixture models. *SPIE Conference Imaging Spectrometry III* (pp. 108–119). [San Diego, CA].
Roberts, D. A., Gardner, M., Church, R., Ustin, S., Scheer, G., & Green, R. O. (1998). Mapping chaparral in the Santa Monica Mountains using multiple endmember spectral mixture models. *Remote Sensing of Environment*, *65*, 267–279.
Rohlf, F. J., & Sokal, R. R. (1981). Statistical tables. (second ed.). New York: W.H. Freeman and Company.
Schaaf, C. B., Gao, F., Strahler, A. H., Lucht, W., Li, X. W., Tsang, T., et al. (2002). First operational BRDF, albedo nadir reflectance products from MODIS. *Remote Sensing Of Environment*, *83*, 135–148.
Shimabukuro, Y. E., & Smith, J. A. (1991). The least-squares mixing models to generate fraction images derived from remote sensing multispectral data. *IEEE Transactions on Geoscience and Remote Sensing*, *N1*, 16–20.
Tucker, C. J. (1979). Red and photographic infrared linear combinations for monitoring vegetation. *Remote Sensing of Environment*, *8*, 127–150.
Tucker, C. J., Dregne, H. E., & Newcomb, W. W. (1991). Expansion and contraction of the Sahara Desert from 1980 to 1990. *Science*, *253*, 299–301.
Warren, P. L., & Hutchinson, C. F. (1984). Indicators of rangeland change and their potential for remote sensing. *Journal of Arid Environments*, *7*, 107–126.
Zhang, X. Y., Friedl, M. A., Schaaf, C. B., Strahler, A. H., Hodges, J. C. F., Gao, F., et al. (2003). Monitoring vegetation phenology using MODIS. *Remote Sensing of Environment*, *84*, 471–475.
Zhang, X. Y., Friedl, M. A., & Schaaf, C. B. (2006). Global vegetation phenology from moderate resolution imaging spectroradiometer (MODIS): Evaluation of global patterns and comparison with in situ measurements. *Journal of Geophysical Research Biogeosciences*, 111.